Soils and Rocks
www.soilsandrocks.com
An International Journal of Geotechnical and Geoenvironmental Engineering
ISSN 1980-9743
ISSN-e 2675-5475

Spread footings bearing on circular and square cement-stabilized sand layers above weakly bonded residual soil

Nilo Cesar Consoli[1,#], Eclesielter Batista Moreira[1], Lucas Festugato[1], Gustavo Dias Miguel[1]

Article

Keywords
Artificially cemented layer
Ground improvement
Lightly bonded residual soil
Spread footings

Abstract
The practice of soil-cement reinforced layers to bear shallow foundations is a feasible option in low bearing capacity soils. This paper addresses the interpretation of plate load tests bearing on compacted artificially cemented sand layers of distinct sizes and shapes (cylindrical and prismatic) overlaying a weakly bonded residual soil stratum. Static load tests were carried out on a rigid circular steel plate (diameter of 300-mm) resting on sand-cement reinforced layers with distinct areas (diameters/widths of 450, 600, and 900-mm) and constant thickness of 300-mm. The results have shown two distinct failure modes that rely on the cemented layer's diameter/width: (a) the steel plate and the artificially cemented layer punch together into the weakly bonded residual soil, without the failure of the cemented layer, and (b) the artificially cemented layer fails. The combination of two traditional methods for predicting bearing capacity in soils was successfully applied considering the shape (and geometry) of the improved layer and the existence (or not) of interaction of the lateral of the cemented layers and the residual soil. Finally, this study highlights the importance of considering the shapes and sizes of soil-cement layers in the bearing capacity estimation (combining analytical solutions) of spread footings resting on treated layers above weakly bonded residual soils.

1. Introduction

In Southern Brazil, urban and industrial developments often take place in terrain where the underlying soils are highly drainable weakly bonded residual soils with high void ratios. These residual soils are usually partly saturated (degree of saturation of about 80 %) and even when saturated, any generated pore pressure is rapidly dissipated. Hence, immediate settlements are more relevant than consolidation settlements in these soils. Such type of material can suffer a high reduction in volume when the bonds are broken. The solution adopted to support significant building loads is usually a deep foundation. However, for some projects, a deep foundation may not be economically feasible. An example is the construction of low-rise, low-cost housing or commercial buildings, where piling costs can represent an unacceptably large proportion of the total investment. The present research studied an alternative to deep foundations: shallow spread footings are placed on an upper layer that has been mechanically improved by incorporation of an engineered cementing material. The approach produces a double-layer foundation system, in which the upper layer has been artificially cemented through mixing, compaction, and curing.

There have been many studies of shallow foundations on layered systems, most of them concentrating on cases in which a sand layer overlies a soft clay stratum (*e.g.*, Meyerhof, 1974; Burd & Frydman, 1997; Kenny & Andrawes, 1997). Only a few (*e.g.*, Vesic, 1975) dealt with cohesive-frictional soils. The accuracy of the Vesic (1975) solution in predicting the ultimate bearing capacity of a footing resting on an artificially cemented upper layer, overlying a weakly bonded residual soil with a high void ratio, is unknown. The stress-strain-strength behavior of artificially cemented soils has been studied in the past by several investigators (*e.g.*, Clough *et al.*, 1981; Coop & Atkinson, 1993; Huang & Airey, 1998; Consoli *et al.*, 2000, 2006,

#Corresponding author. E-mail address: consoli@ufrgs.br.
[1]Programa de Pós-Graduação em Engenharia Civil, Universidade Federal do Rio Grande do Sul, Porto Alegre, RS, Brazil.

Submitted on May 28, 2020; Final Acceptance on July 6, 2020; Discussion open until December 31, 2020.
DOI: https://doi.org/10.28927/SR.433339

2008, 2009, 2010, 2011, 2012, 2013, 2014, 2015, 2016, 2017, 2018, 2019, 2020a, b, c; Dalla Rosa *et al.*, 2008).

Foppa *et al.* (2020) and Caballero (2019) observed, in small scale load tests of footings resting on a soil-cement reinforced layer over a loose sand, two distinct types of failure: in the first, the reinforcement layer is punched through the soil, without showing any fissuring, up to a settlement corresponding to the natural soil bearing capacity. In the second, after an initial settlement, the reinforced layer breaks, showing a fissure that may be located near the edge or at the footing's center axis, which propagates upwards as the settlement continues.

The main purpose of the present research is to investigate the response of compacted soil-cement layers, with distinct geometries and resting on a weak cohesive frictional soil, to field plate loads. The system failure modes, load-displacement characteristics and bearing capacity prediction are also addressed.

2. Experimental program

The experimental program was carried out in three stages. Firstly, the materials characterization was performed. Then, mechanical properties of molded specimens were determined through consolidated drained triaxial tests, including the stress-strain behavior of the natural soil and the cemented mixture. Finally, plate load tests were performed directly on the residual soil and on the improved layers, considering distinct layer diameters (D_r) and edges (L_r), with and without side friction and with the same thicknesses (H_r), which allowed the assessment of the influence of the reinforcement layer area and side friction (adhesion) on the load capacity, as well as the failure modes of the foundation system.

2.1 Weakly bonded (cohesive-frictional) residual soil site

The features of the residual soil at the experimental site have been determined by *in situ* cone penetration tests (CPT). The CPT soil profile, to a depth of 7 m, is portrayed in Fig. 1. The CPT data shows a soil crust with less than 1 m, with tip resistance (q_c) reaching 4.8 MPa, overlaying a 3 m layer with q_c of approximately 1.0 MPa, and a 3 m layer with a maximum q_c of 1.7 MPa. The side friction (f_s) follows a similar pattern.

From a sample retrieved from a depth of 2.0 m, it was possible to determine the particle size distribution, showing 2.0 % medium sand (0.425 mm and 2.0 mm), 20.0 % fine sand (0.075 mm and 0.425 mm), 22.0 % silt (0.002 mm and 0.075 mm) and 56.0 % of clay (≤ 0.002 mm). The liquid limit and plasticity index were determined to be 42 % and 11 %, respectively, with the natural moisture content at 33 %. According to the USCS (ASTM 2017) the soil was classified as a lean clay with sand - CL. The unit weight of the solid grains is 26.7 kN/m^3, while the average bulk unit weight and the dry unit weight were determined to be 16.1 kN/m^3 and 12.1 kN/m^3, respectively. Finally, a void ratio 1.21 and a degree of saturation 73 % were also determined. The unconfined compressive strength, determined after the specimens were immersed in water for 24 h, was 89 kPa (average value), varying between 84 kPa (minimum value) and 92 kPa (maximum value). The hydraulic conductivity is relatively high at 1.1×10^{-5} m/s.

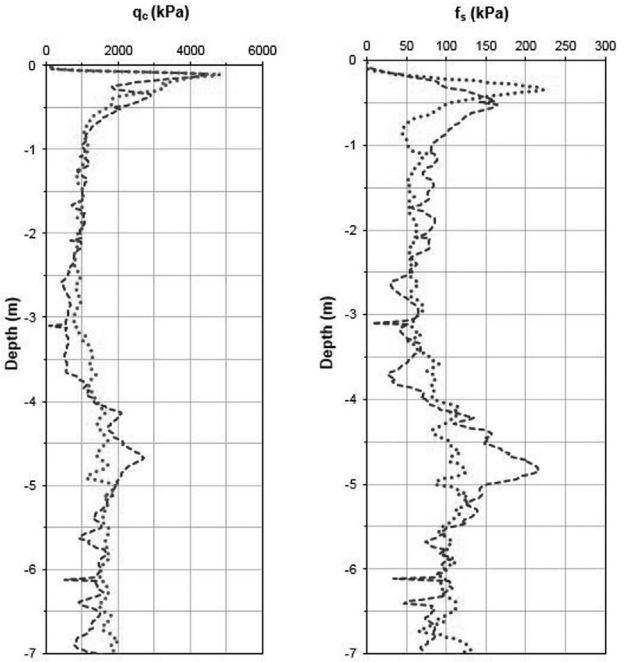

Figure 1. CPT soil profiles to a depth of 7-m.

Stress-strain curves obtained from drained triaxial tests of fully saturated undisturbed specimens, under confining pressures of 20, 60 and 100 kPa, are shown in Fig. 2. The 20 kPa confining pressure test revealed a small strain stiffness of 49 MPa and a Poisson coefficient (v) of 0.15 (after a strain of 0.01 %, measured with Hall effect sensors). The reduction in soil stiffness for the higher confining pressures - 60 and 100 kPa - is not surprising in such lightly bonded soils, due to the changes in fabrics produced by the elimination of the cementation at the particles' contact points, caused by the increased confining pressures (Leroueil & Vaughan, 1990; Consoli *et al.*, 1998, 2000, 2006). All the axial strain-volumetric strain curves present contractive behavior (Fig. 2b). The failure envelope presents an effective peak friction angle (ϕ') of 31.8° and an effective cohesion intercept (c') of 23.8 kPa.

In addition, as the naturally bonded soil in the field is partly saturated (S_r = 73 %), the matric suction was assessed through the filter paper technique described by the ASTM D5298 standard (ASTM, 2003) using a Whatman grade 42 filter paper (Chandler *et al.*, 1992, Marinho & Oliveira, 2006). Considering the field conditions (moisture content and degree of saturation), the average matric suction was estimated at 8.8 kPa (varying between 4 and 10 kPa), which corresponds to less than 10 % of the unconfined compressive strength of the natural soil.

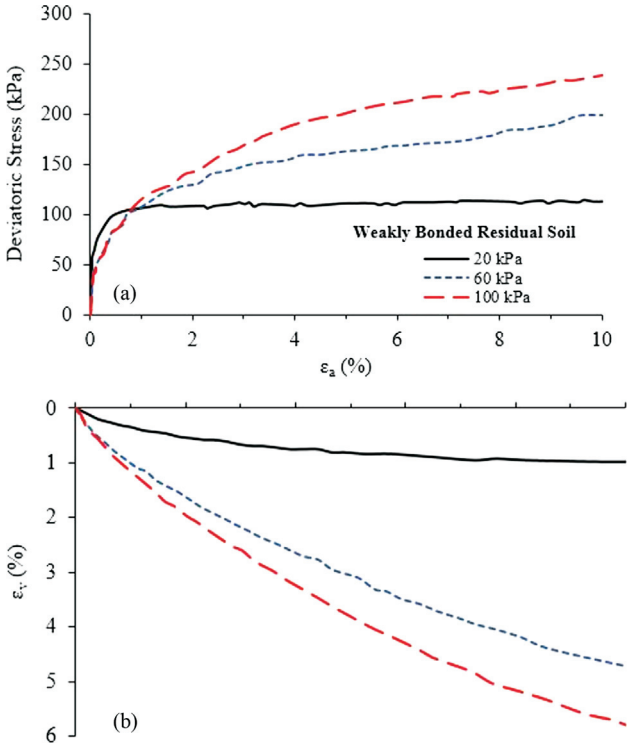

Figure 2. Saturated drained conventional triaxial tests at confining stresses of 20, 60 and 100-kPa for bonded residual soil: (a) deviator stress *vs.* ε_a and (b) ε_v *vs.* ε_a.

2.2 Artificially cemented field layers

The artificially cemented field layers prepared in the present research were composed of Osório sand blended with 5 % Portland cement (in percentage of the dry sand). The percentage of Portland cement was chosen considering the international and Brazilian experience with soil-cement (*e.g.*, Ingles & Metcalf, 1972, Mitchell, 1981, Consoli *et al.*, 2009) in experimental and practical works. Water was added to the mixtures to obtain overall water content of 10 % (Consoli *et al.*, 2010) and the mixing continued until a homogeneous paste was acquired. The sand used is eolic, quartzitic, free of organic matter, non-plastic, and obtained from the Osório region in the province of Rio Grande do Sul, Brazil. The sand properties are listed in Table 1. According to ASTM (2017), the soil is classified as poorly graded sand (SP). Early high strength Portland cement [Type III - ASTM (2019)] was used as a cementation agent. Its fast gain of strength allowed a curing period of 28 days for the field trials (as well as the samples collected in the field for laboratory trials). The specific gravity of cement grains is 3.05. Tap water was employed all over this study.

Six circular and three square artificially cemented Osório sand layers were built on the surface of the residual soil site. The circular layers were built with diameters (D_r) of 450, 600, and 900 mm and a thickness (H_r) of 300 mm, while square layers were built with widths (L_r) of 450, 600, and 900 mm, also with a thickness of 300 mm. The typical test configuration describing the improved soil layers is presented in Fig. 3. Before mixing and compaction of the upper-cemented layers, a 500 mm thick layer, of local residual soil, was removed from the test area and the pit was dug according to the specified dimensions of each circular and square layer (see Table 2). Each cemented layer was compacted in several sub-layers, by manual compaction, until the specified 300 mm thickness was achieved. The final layer had a pre-determined dry unit weight of 15.4kN/m^3 (void ratio of 0.70), and was left to cure for 28 days, prior to the field loading tests.

Table 1. Physical properties of the studied soils.

Properties	Residual soil	Osório sand
Specific gravity	2.67	2.63
Medium sand (0.425 mm < diameter < 2.0 mm): %	2.0	0.3
Fine sand (0.075 mm < diameter < 0.425 mm): %	20.0	97.6
Silt (0.002 mm < diameter < 0.075 mm): %	22.0	1.6
Clay (diameter < 0.002 mm): %	56.0	0.5
Liquid limit	42.0	-
Plastic index	11.0	Non-plastic
Soil classification (ASTM, 2017)	CL	SP

After curing, and immediately before the test, the natural residual soil in contact with the lateral of the treated layers, coded D_r450H_r300, D_r600H_r300 and D_r900H_r300, was removed, so that these results could be compared with those obtained by the layers which were left in contact with the lateral soil. The mechanical parameters of the artificially cemented layers were acquired through conventional saturated drained triaxial tests, isotropically consolidated under effective confining pressures of 20, 40 and 100 kPa (Fig. 4), performed on undisturbed specimens directly collected from the stabilized slabs, after the 28-days curing period. The 20 kPa confining pressure triaxial result presents a small strain Young modulus of 3,430 MPa and a Poisson coefficient (v) of about 0.2 (measured after 0.01 % strains, using Hall effect sensors). The stress-strain response of all tests, regardless of the confining stress, shows a linear response, up to peak, followed by a brittle and strain softening behavior (Fig. 4a). The results led to a peak friction angle (ϕ') of 36.4° and a cohesion intercept (c') of 145.5 kPa.

2.3 Spread footing testing program

The field tests were performed based on the contents of ABNT NBR 6489 (2019). The load (Q) was applied by a hydraulic jack reacting on a structural loaded beam and was measured by a calibrated 500 kN load cell. To measure the

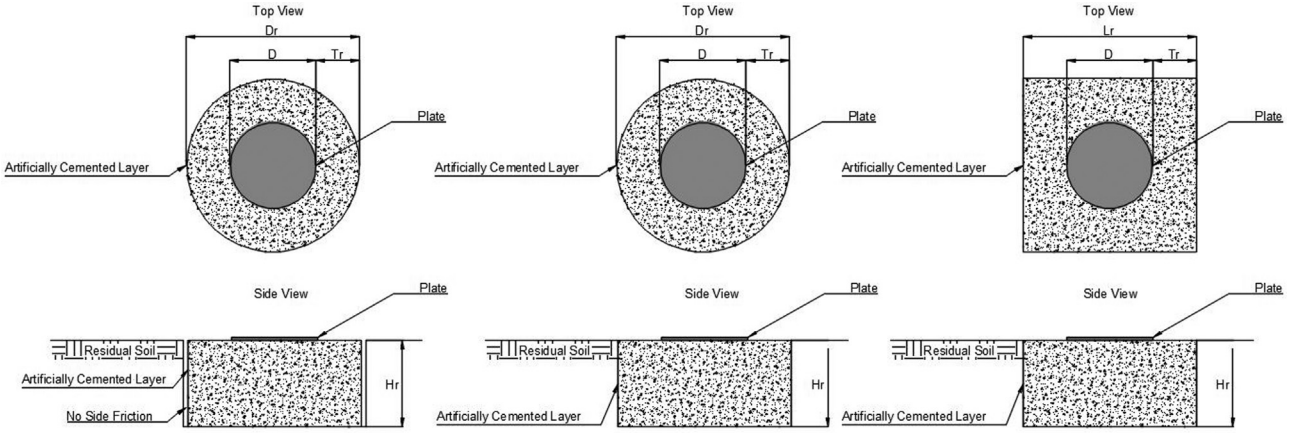

Figure 3. Tests setup depicting the improved soil layers: (a) improved soil circular layers without side friction; (b) improved soil circular layers with side friction; (c) improved soil square layers with side friction.

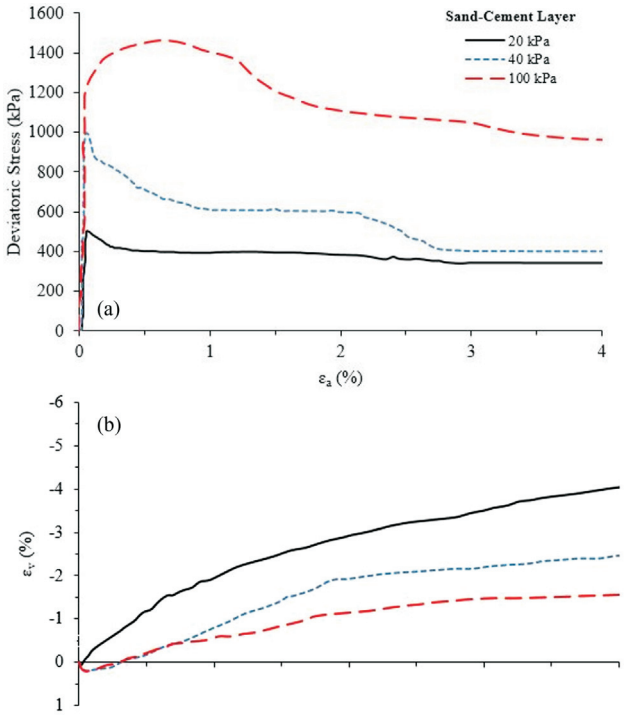

Figure 4. Artificially cemented layers CID tests at confining stresses of 20, 40 and 100-kPa: (a) deviator stress *vs.* axial strain (ε_a) and, (b) volumetric strain (ε_v) *vs.* axial strain (ε_a).

vertical displacement, three dial gauges, with a 0.01 mm resolution and 50 mm course, were installed at the top of the plate, on an equilateral triangle pattern. The devices were installed on a supporting beam and fixated by peripheral rods. The load was applied in similar increments of less than one tenth of the expected bearing capacity. The failure load (Q_u) was assumed to be that corresponding to a relative displacement (δ/D) of 3.0 %. Such failure criterion was suggested by Consoli *et al.* (2009), based on previous studies of more than 200 spread footings carried out by Berardi & Lancellotta (1991).

The spread footing testing program comprises twelve spread footing tests (see Table 2). Three spread footing tests were carried out using 300, 600, and 900 mm diameter rigid steel footings, directly on the residual soil, after the removal of the 500 mm upper layer of the local crust. Nine further spread footing tests were carried out using 300 mm diameter rigid footings, on the sand-cement layers (Table 2).

3. Spread footing testing results and analysis

Figure 5 presents results of applied load *vs.* vertical displacements of the twelve spread footing tests carried out in the present research. Looking first at the results of the three footing tests [300-mm diameter (coded D300), 600-mm diameter (coded D600) and 900-mm diameter (coded D900)] bearing directly on the weakly bonded residual soil, it can be observed that at a given settlement, higher loads are related to larger footing diameter (and consequently larger areas of the footings). Punching failure of the residual soil at the edge of the circular steel footings was observed in all three tests carried out, regardless of the footing diameter. Looking now to the results of the three 300-mm diameter steel footing tests bearing on sand-Portland cement field circular and square layers [with diameters of 450, 600 and 900-mm both with and no side friction, coded D_r450H_r300, D_r600H_r300, D_r900H_r300 (for circular layers without side friction), coded D_r450H_r300 - SF, D_r600H_r300 - SF, D_r900H_r300 SF (for circular layers with side friction) and coded L_r450H_r300, L_r600H_r300, L_r600H_r300 (for square layers with side friction) - see Table 2] over the weakly bonded residual soil, it can be observed that for a given settlement higher loads were observed for larger artificially cemented sand field layers. However, there are distinct failure mechanisms according to the diameter/width of the sand-Portland cement layers.

Table 2. Artificially cemented layer field dimensions, strength of cemented layer field specimens.

Test	Code	Diameter of the circular steel plate - D (mm)	Geometric form	Treated layer		H/D	Note
				Diameter or width - D_r or L_r (mm)	Thickness - H_r (mm)		
1	D300	300	-	-	-	-	Natural Soil
2	D600	600	-	-	-	-	Natural Soil
3	D900	900	-	-	-	-	Natural Soil
4	D_r450H_r300	300	Circular	450	300	1	No side friction
5	D_r600H_r300	300	Circular	600	300	1	No side friction
6	D_r900H_r300	300	Circular	900	300	1	No side friction
7	D_r450H_r300 - SF	300	Circular	450	300	1	Side Friction
8	D_r600H_r300 - SF	300	Circular	600	300	1	Side Friction
9	D_r900H_r300 - SF	300	Circular	900	300	1	Side Friction
10	L_r450H_r300 - SF	300	Square	450	300	1	Side Friction
11	L_r600H_r300 - SF	300	Square	600	300	1	Side Friction
12	L_r900H_r300 - SF	300	Square	900	300	1	Side Friction

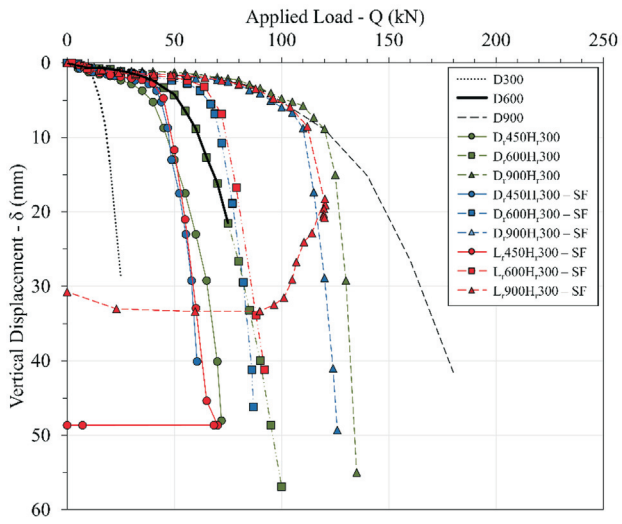

Figure 5. Load-settlement curves of 300-mm diameter (coded D300), 600-mm diameter (coded D600) and 900-mm diameter (coded D900) circular steel footing bearing on weakly bonded residual soil, and 300-mm diameter circular steel footing bearing on 450, 600 and 900-mm diameter treated layer without side friction (coded D_r450H_r300, D_r600H_r300 and D_r900H_r300), 450, 600 and 900-mm diameter treated layer with side friction (coded D_r450H_r300 - SF, D_r600H_r300 - SF and D_r900H_r300 - SF) and, 450, 600 and 900-mm widths treated layer with side friction (coded L_r450H_r300, L_r600H_r300 and L_r900H_r300) of artificially cemented sand layers over weakly bonded residual soil.

Punching failure of the residual soil was observed at the edge of the sand-cement field layers with 450 mm in diameter and a 450 mm side (coded D_r450H_r300, coded D_r450H_r300 - SF and L_r450H_r300 - SF) and 600 mm in diameter and 600 mm square (coded D_r600H_r300, coded D_r600H_r300 - SF and L_r600H_r300 - SF), as if these six treated layers were part of the shallow foundation structure. This failure mechanism was corroborated by the field analysis of the treated layers after the end of the test, since no cracks or fractures were observed in such layers (see photo of the intact treated circular and square layer with 450 mm diameter and width, respectively and, 300 mm thick retrieved from the field in Fig 6).

For punching failure, as the load increases, there is breakage of the bonds of the weakly bonded residual soil below the spread footing structure, and vertical continuous penetration of the footing structure, with virtually no lateral soil movement. On the other hand, after a certain vertical load (Q) was applied to the 300 mm diameter rigid circular steel plate bearing on the sand-cement layers of 900 mm diameter (D_r900H_r300), 900 mm diameter with side friction (D_r900H_r300 - SF) and 900 mm square (L_r900H_r300 - SF), there was a failure of such artificially cemented layers after reaching certain Q. This mode of failure (fracturing of the layers) was attested by the cracks found in the cylindrical and prismatic volume that was cut vertically after completion of the load test [see photos of the failed layer of 900 mm diameter (D_r900H_r300) in Fig. 7 and of 900 mm width (L_r900H_r300 - SF) in Fig. 8]. Consoli *et al.* (2009) observed similar failures for the infinite cemented layers. These authors also verified, by means of finite element method simulations, that tensile cracks start at the bottom of the cemented soil layer, below the circular plates.

Looking back to Fig. 5, it is possible to observe that applied load (Q) *vs.* vertical displacement (δ) curves of the tests D600 and D_r600H_r300 are identical. Such similarity is not a coincidence, since D600 (a circular steel footing of

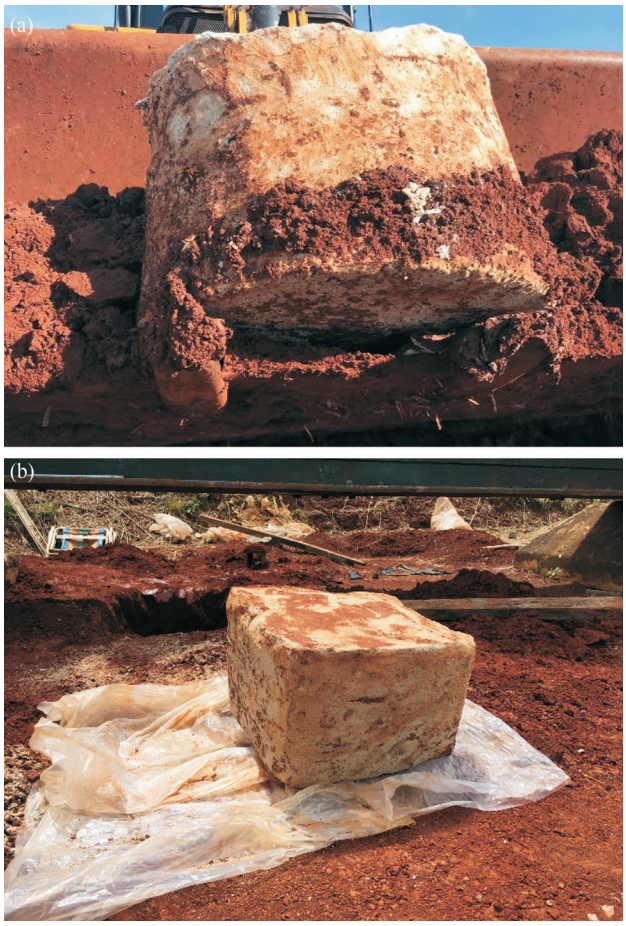

Figure 6. Improved sand-Portland cement retrieved from the field: (a) Cylindrical shape of the 450-mm diameter and 300-mm thick (coded D_r450H_r300); and (b) Prismatic shape of the 450-mm square and 300-mm thick (coded L_r450H_r300 - SF).

Figure 7. Photos of the (a) general view and (b) vertical cut in the middle of the 900-mm diameter and 300-mm thick Portland cement improved sand layer (coded D_r900H_r300) to check failure mechanism below the steel plate vertically loaded.

600 mm diameter) is distributing its load through the same area of the base of the D_r600H_r300 test, with a circular footing of 300 mm diameter, bearing on a sand-cement field layer with 600 mm diameter and 300 mm thick, that is kept intact until the end of the test. In other words, the sand-cement field layer with 600 mm diameter and 300 mm thick is acting as if it is part of the shallow foundation structure of a circular footing of 600 mm diameter. So, in reality, D600 and D_r600H_r300 spread footing tests have a similar base regarding the transfer of the vertical stresses to the residual soil. However, the same does not happen for the sand-cement circular and square layers coded D_r600H_r300 - SF and L_r600H_r300 - SF, because the side friction (and adhesion) increases their bearing capacity. It can also be noticed that the bearing capacity of the sand-cement square layer (L_r600H_r300 - SF) is slightly larger than the sand-cement circular layer (D_r600H_r300 - SF) due to the area and perimeter of the square layer being larger than the circular layer. Also, in Fig. 5, it can be observed that the applied load (Q) *vs*. vertical displacement (δ) curves of spread footing tests D900 and D_r900H_r300 are coincident only up to a certain load. Such situation is also not a coincidence, since D900 (a circular steel footing of 900 mm diameter) is distributing its load through to the same area of the D_r900H_r300, up to a point of fracturing the artificially cemented layer. After the failure of the sand-cement field layer starts to occur, the two Q *vs*. δ curves separate from each other.

Based on studies by Consoli *et al.* (1998), the applied load (Q) *vs*. vertical displacements (δ) curves are normalized by dividing Q by the foundation-residual soil contact area [named equivalent stress (σ_{eq})] and δ by the diameter of the foundation-residual soil contact area (D_r), named relative displacement (δ/D_r). Fig. 9 presents the normalized results of the three circular steel footing tests bearing directly on the weakly bonded residual soil (coded D300, D600 and D900), which ends up in a unique curve. Normalized σ_{eq} *vs.* δ/D_r results for the two shallow foundation tests bearing on improved layers that failed by punching (coded D_r450H_r300 and D_r600H_r300, in which the steel footing plus the Portland cement improved layers behaved as a sin-

Figure 8. Photos of (a) the top view and (b) vertical cut in the middle of the 900-mm square and 300-mm thick Portland cement improved sand layer (coded L_r900H_r300 - SF) to check failure mechanism below the steel plate vertically loaded.

gle shallow foundation resting on the bonded residual soil, also maintained their behavior similar to the tests performed directly on the natural bonded residual soil. However, the same does not happen for the normalized σ_{eq} *vs.* δ/D_r results of the sand-cement field circular layers (coded D_r450H_r300 - SF and D_r600H_r300 - SF) and square layers (coded L_r450H_r300- SF and L_r600H_r300 - SF), once the side friction (and adhesion) further enhances their behavior at

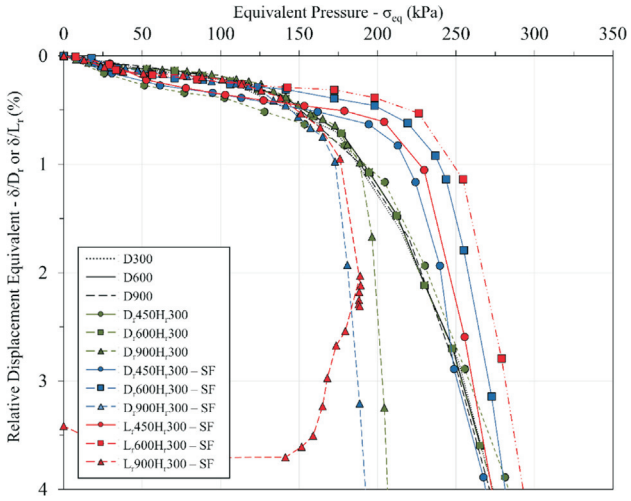

Figure 9. Equivalent pressure (σ_{eq}) *vs.* relative displacement (δ/D_r or δ/L_r) curves of 300 mm, 600 mm and 900 mm diameter circular steel footing bearing on weakly bonded residual soil, and 300 mm diameter circular steel footing bearing on 450, 600 and 900-mm diameter treated layer without side friction (coded D_r450H_r300, D_r600H_r300 and D_r900H_r300), 450, 600 and 900 diameter treated layer with side friction (coded D_r450H_r300 - SF, D_r600H_r300 - SF and D_r900H_r300 - SF) and, 450, 600 and 900 widths treated layer with side friction (coded L_r450H_r300 - SF, L_r600H_r300 - SF and L_r900H_r300 - SF) of artificially cemented sand layers over weakly bonded residual soil.

small relative displacements. The normalized σ_{eq} *vs.* δ/D_r curve of D_r900H_r300 shallow foundation test is also similar (practically the same "unique" curve based on the previous normalized results) up to the occurrence of the extensive cracking of the improved layer, whose macroscopic sequel clearly starts at a relative displacement (δ/D_r) of about 1.0 % (see Fig. 9). After such point, the normalized σ_{eq} *vs.* δ/D_r curve of D_r900H_r300 shallow foundation test diverge from the "unique" general normalized curve. Related behavior is followed by tests coded D_r900H_r300 - SF and L_r900H_r300 - SF.

Figure 10 and Table 3 show the field failure load (Q_u) results (in a space diameter of the cement treated sand layer *vs*. failure load) and analytical solutions based on the Hansen (1961) and Vesic (1975) theories in a unique graph. It is expected that the results where soil punching occurred could be determined using standard analytical bearing capacity theory of Hansen (1961), while that in the three cases [900 mm diameter and square (coded D_r900H_r300, D_r900H_r300 - SF and L_r900H_r300 - SF)] where the failure mode prediction is the occurrence of failure of the artificially cemented layer, the Vesic (1975) bearing capacity theory of double layer is expected to give good results up to H_r/D = 1.0 (Consoli *et al.*, 2008). The Hansen (1961) method [Eq. (1)] was applied as if the structural foundation was a single element (steel footing plus cement improved sand layer) resting on weakly bonded residual soil. The

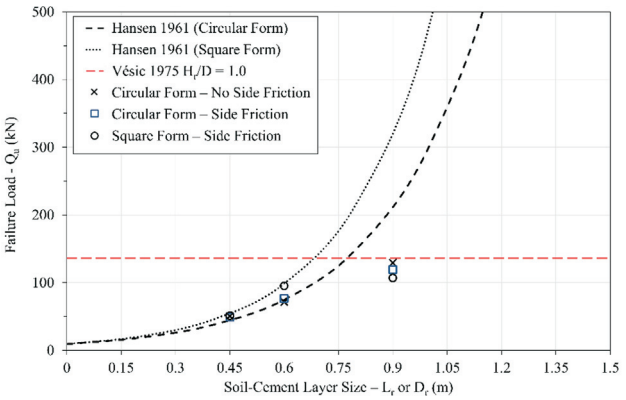

Figure 10. Bearing capacity of square and circular shallow foundations prediction considering soil cement layer as a part of the foundation (Hansen, 1961) and considering it as an infinite treated layer with H_r/D = 1.0 (Vesic, 1975).

strength parameters of the weakly bonded residual soil were reduced to a lower limit value of 2/3 in order to agree with Terzaghi (1943) recommendations for punching failure mechanisms (Consoli *et al.*, 1998).

$$\frac{Q_u}{A_c} = c' N_c S_c + \frac{D_r}{2} \gamma N_\gamma S_\gamma \quad (1)$$

where A_c is the area of the cemented layer, D_r is the diameter of the improved layer, γ is the unit weight of the residual soil; N_c, N_γ are the bearing capacity factors; and S_c, S_γ are the shape factors for circular and square foundations, given by

$$N_c = \left[e^{\pi \tan \phi'} \tan^2 \left(45° + \frac{\phi'}{2} \right) - 1 \right] \cot \phi' \quad (2)$$

$$N_\gamma = 2 \left[e^{\pi \tan \phi'} \tan^2 \left(45° + \frac{\phi'}{2} \right) + 1 \right] \tan \phi' \quad (3)$$

$$S_c = 1 + \frac{e^{\pi \tan \phi'} \tan^2 \left(45° + \frac{\phi'}{2} \right)}{\left(e^{\pi \tan \phi'} \tan^2 \left(45° + \frac{\phi'}{2} \right) - 1 \right) \cot \phi'} \quad (4)$$

$$S_\gamma = 0.6 \quad (5)$$

The Vesic (1975) solution [Eq. (6)] establishes the bearing capacity of a footing resting on an infinite upper cement-sand layer with strength parameters c_1' and ϕ_1' superposed to a lower (bonded residual soil) weak layer with strength parameters c_2' and ϕ_2' (involving both cohesion and friction strength parameters) as:

Table 3. Field and analytical failure loads (Q_u) and failure modes of shallow foundations bearing on cement treated layers.

D_r or L_r (m)	Q_u (kN) - at δ/D = 3 %				$Q_{ur(t)}$ (kN) - Hansen (1961)		$Q_{ur(t)}$ (kN) - Vésic (1975)	Prevision	Field result
	Circular		Square		Circular	Square			
	No side friction	Side friction	Side friction						
0.45	50.6	49.1	51.0		47.0	57.1	-	Punching	Punching
0.60	71.7	76.6	95.3		84.8	103.2	-	Punching	Punching
0.90	129.2	119.2	106.9		-	-	136.2	Cemented layer generalized failure	Cemented layer generalized failure

$$\frac{Q_u}{A_c} = \left[q_0 + \left(\frac{1}{\frac{1-(\sin\phi_1')^2}{1+(\sin\phi_1')^2}} \right) c_1' \cot\phi_1' \right] \times e^{4\frac{1-(\sin\phi_1)^2}{1+(\sin\phi_1)^2}\tan\phi_1\left(\frac{H_r}{D_r}\right)} - \left(\frac{1}{\frac{1-(\sin\phi_1')^2}{1+(\sin\phi_1')^2}} \right) c_1' \cot\phi' \quad (6)$$

where A_s is the area of the steel plate, q_0 is the bearing capacity as if the spread footing was resting on the top of the natural soil, considering the reduction in the strength parameters for punching the failure mechanism.

From Fig. 10, it is possible to notice that the bearing capacity prediction considering the cement treated sand layer is a fine analytical solution when considering as a part of the shallow foundation. Such solution threshold is given by the cement treated layer (Vesic, 1975) solution, for specific H_r/D. The composition of the two analytical solutions described above has shown to be a useful tool to predict the failure behavior of cement treated sand layers resting above the weakly bonded residual soil.

4. Conclusions

This study evaluated the behavior of circular steel plates bearing on distinct diameters and widths cement treated sand layers, maintaining the same thicknesses, on weakly bonded residual soil site. From the data gathered from the present study, the following conclusions can be portrayed:

- Two distinct modes of rupture were observed in the present field study, depending on the diameter or widths of sand-Portland cement blend. For the sand-Portland cement layers diameters and widths up to 600 mm, the limit load was successfully evaluated as if the improved layers worked in association with the circular steel foundation, as a foundation transferring its load directly to the weakly bonded residual soil (which fails due to punching), once no cracking or fissuring were observed in the artificially cemented layer. The reinforced layers of diameter (or width) of 900 mm broke due to the excessive tensile stresses that were developed in the bottom of the cemented layer. Therefore, the carrying capacity of the circular plate supported in this layer can be evaluated as if this layer were "infinite" or continuous;
- A single curve in σ_{eq} *vs.* δ/D_r space is achieved when plotting the spread footing field tests performed, with and without improved layer, up to the rupture of the treated layer (when applicable);
- The combined use of Hansen (1961) and Vesic (1975) analytical solutions proved to be a useful way to predict the failure behavior and the bearing capacity of cement treated layers of distinct shapes bearing on weakly bonded residual soil site.

Acknowledgments

The authors wish to explicit their appreciation to MCT-CNPq (Editais INCT, Universal & Produtividade em Pesquisa), FAPERGS/CNPq 12/2014 - PRONEX (Project # 16/2551-0000469-2), and MEC-CAPES (PROEX) for the support to the research group.

References

ABNT (2019). Soil - Static Load Test on Shallow Foundation - NBR 6489. Associação Brasileira de Normas Técnicas, São Paulo, Brazil.

ASTM (2003). Standard Test Method for Measurement of Soil Potential (Suction) Using Filter Paper - ASTM D5298. ASTM International, West Conshohocken, Philadelphia, USA.

ASTM (2017). Standard Practice for Classification of Soils for Engineering Purposes (Unified Soil Classification System) - ASTM D2487. ASTM International, West Conshohocken, Philadelphia, USA.

ASTM (2019). Standard Specification for Portland Cement - ASTM C150. ASTM International, West Conshohocken, Philadelphia, USA.

Berardi, R. & Lancellotta, R. (1991). Stiffness of granular soil from field performance. Géotechnique, 41(1):149-157. https://doi.org/10.1680/geot.1991.41.1.149

Burd, J. & Frydman, S. (1997). Bearing capacity of plane-strain footings on layered soil. Canadian Geotechnical Journal, 34(2):241-253. https://doi.org/10.1139/t96-106

Caballero, R.D. (2019). Desenvolvimento de uma Metodologia de Projeto de Fundações Superficiais Circulares Assentes Sobre Camada de Solo-Cimento. M.Sc. Dissertation, Programa de Pós-Graduação em Engenharia Civil, Universidade Federal do Rio Grande do Sul, Porto Alegre, Brasil, 198 p. (in Portuguese). https://lume.ufrgs.br/handle/10183/194594.

Chandler, R.J.; Crilly, M.S. & Montgomery-Smith, G. (1992). A low-cost method of assessing clay desiccation for low-rise buildings. Proceedings of the Institution of Civil Engineers - Civil Engineering, 92(2):82-89. https://doi.org/10.1680/icien.1995.27840

Clough, G.W.; Sitar, N.; Bachus, R.C. & Rad, N.S. (1981). Cemented sands under static loading. Journal of Geotechnical Engineering Division, 107(6):799-817.

Consoli, N.C.; Schnaid, F. & Milititsky, J. (1998). Interpretation of plate load tests on residual soil site. Journal of Geotechnical and Geoenvironmental Engineering, 124(9):857-867. https://doi.org/10.1061/(ASCE)1090-0241(1998)124:9(857)

Consoli, N.C.; Rotta, G.V. & Prietto, P.D.M. (2000). Influence of curing under stress on the triaxial response of

cemented soils. Géotechnique, 50(1):99-105. https://doi.org/10.1680/geot.2000.50.1.99

Consoli, N.C.; Rotta, G.V. & Prietto, P.D.M. (2006). Yielding-compressibility-strength relationship for an artificially cemented soil cured under stress. Géotechnique, 56(1):69-72. https://doi.org/10.1680/geot.2006.56.1.69

Consoli, N.C.; Thomé, A.; Donato, M. & Graham, J. (2008). Loading tests on compacted soil, bottom-ash and lime layers. Proceedings of the Institution of Civil Engineers - Geotechnical Engineering, 161(1):29-38. https://doi.org/10.1680/geng.2008.161.1.29

Consoli, N.C.; Dalla Rosa, F. & Fonini, A. (2009). Plate load tests on cemented soil layers overlying weaker soil. Journal of Geotechnical and Geoenvironmental Engineering, 135(12):1846-1856. https://doi.org/10.1061/(ASCE)GT.1943-5606.0000158

Consoli, N.C.; Cruz, R.C.; Floss, M.F. & Festugato, L. (2010). Parameters controlling tensile and compressive strength of artificially cemented sand. Journal of Geotechnical and Geoenvironmental Engineering, 136(5):759-763. https://doi.org/10.1061/(ASCE)GT.1943-5606.0000278

Consoli, N.C.; Cruz, R.C. & Floss, M.F. (2011). Variables controlling strength of artificially cemented sand: Influence of curing time. Journal of Materials in Civil Engineering, 23(5):692-696. https://doi.org/10.1061/(ASCE)MT.1943-5533.0000205

Consoli, N.C.; Cruz, R.C.; Viana da Fonseca, A. & Coop, M.R. (2012). Influence of cement-voids ratio on stress-dilatancy behavior of artificially cemented sand. Journal of Geotechnical and Geoenvironmental Engineering, 138(1):100-109. https://doi.org/10.1061/(ASCE)GT.1943-5606.0000565

Consoli, N.C.; Festugato, L.; Da Rocha, C.G. & Cruz, R.C. (2013). Key parameters for strength control of rammed sand-cement mixtures: Influence of types of Portland cement. Construction and Building Materials, 49:591-597. https://doi.org/10.1016/j.conbuildmat.2013.08.062

Consoli, N.C.; Lopes Jr., L.S.; Consoli, B.S. & Festugato, L. (2014). Mohr-Coulomb failure envelopes of lime-treated soils. Géotechnique, 64(2):165-170. https://doi.org/10.1680/geot.12.P.168

Consoli, N.C.; Festugato, L.; Consoli, B.S. & Lopes Jr., L.S. (2015). Assessing failure envelopes of soil-fly ash-lime blends. Journal of Materials in Civil Engineering, 26(9):04014174. https://doi.org/10.1061/(ASCE)MT.1943-5533.0001134

Consoli, N.C.; Quiñónez Samaniego, R.A.; Marques, S.F.V.; Venson, G.I.; Pasche, E. & González Velázquez, L.E. (2016). A single model establishing strength of dispersive clay treated with distinctive binders. Canadian Geotechnical Journal, 53(12):2072-2079. https://doi.org/10.1139/cgj-2015-0606

Consoli, N.C.; Marques, S.F.V.; Floss, M.F. & Festugato, L. (2017). Broad-spectrum empirical correlation determining tensile and compressive strength of cement-bonded clean granular soils. Journal of Materials in Civil Engineering, 29(6):06017004. https://doi.org/10.1061/(ASCE)MT.1943-5533.0001858

Consoli, N.C.; da Silva, A.P.; Nierwinski, H.P. & Sosnoski, J. (2018). Durability, strength, and stiffness of compacted gold tailings - cement mixes. Canadian Geotechnical Journal, 55(4):486-494. https://doi.org/10.1139/cgj-2016-0391

Consoli, N.C.; Leon, H.B.; Carretta, M.S.; Daronco, J.V.L. & Lourenço, D.E. (2019). The effects of curing time and temperature on stiffness, strength and durability of sand environment friendly binder blends. Soils and Foundations, 59(2):1428-1439. https://doi.org/10.1016/j.sandf.2019.06.007

Consoli, N.C.; Festugato, L.; Scheuermann Filho, H.C.; Miguel, G.D.; Tebechrani Neto, A. & Andreghetto, D. (2020a). Durability assessment of soil-pozzolan-lime blends through ultrasonic pulse velocity test. Journal of Materials in Civil Engineering, 32(8):04020223. https://doi.org/10.1061/(ASCE)MT.1943-5533.0003298

Consoli, N.C.; Bittar Marin, E.J.; Quiñónez Samaniego, R.A.; Scheuermann Filho, H.C. & Cristelo, N.M.C. (2020b). Field and laboratory behaviour of fine-grained soil stabilized with lime. Canadian Geotechnical Journal, 57(6):933-938. https://doi.org/10.1139/cgj-2019-0271

Consoli, N.C.; Carretta, M.S.; Festugato, L.; Leon, H.B.; Tomasi, L.F. & Heineck, K.S. (2020c). Ground waste glass-carbide lime as a sustainable binder stabilising three different silica sands. Géotechnique, *in press*. https://doi.org/10.1680/jgeot.18.P.099

Coop, M.R. & Atkinson, J.H. (1993). The mechanics of cemented carbonate sands. Géotechnique, 43(1):53-67. https://doi.org/10.1680/geot.1993.43.1.53

Dalla Rosa, F.; Consoli, N.C. & Baudet, B.A. (2008). An experimental investigation of the behaviour of artificially cemented soil cured under stress. Géotechnique, 58(8):675-679. https://doi.org/10.1680/geot.2008.58.8.675.

Foppa, D.; Sacco, R.L. & Consoli, N.C. (2020). Bearing capacity of footings on an artificially cemented layer above weak foundation layer. Proceedings of the Institution of Civil Engineers - Ground Improvement, *in press*. https://doi.org/ 10.1680/jgrim.18.00089

Hansen, J.B. (1961). A general formula for bearing capacity. Bulletin No. 11, pp. 38-46. Copenhagen, Denmark: Danish Geotechnical Institute.

Huang, J.T. & Airey, D. (1998). Properties of artificially cemented carbonate sand. Journal of Geotechnical and Geoenvironmental Engineering, 124(6):492-499. https://doi.org/10.1061/(ASCE)1090-0241(1998)124:6(492)

Ingles, O.G. & Metcalf, J.B. (1972). Soil Stabilization: Principles and Practice. Butterworths, Sydney.

Kenny, M.J. & Andrawes, K.Z. (1997). The bearing capacity of footing on sand layer overlying soft clay. Géotechnique, 47(2):339-345. https://doi.org/10.1680/geot.1997.47.2.339

Leroueil, S. & Vaughan, P.R. (1990). The general and congruent effects of structure in natural soils and weak rocks. Géotechnique, 40(3):467-488. https://doi.org/10.1680/geot.1990.40.3.467

Marinho, F.A.M. & Oliveira, O.M. (2006). The filter paper method revisited. Geotechnical Testing Journal, 29(3):250-258. https://doi.org/10.1520/GTJ14125

Meyerhof, G.G. (1974). Ultimate bearing capacity of footings on sand layer overlying clay. Canadian Geotechnical Journal, 11(2):223-229. https://doi.org/10.1139/t74-018

Mitchell, J.K. (1981). Soil improvement - State of the art report. Proc. 10th Int. Conf. on Soil Mechanics and Foundation Engineering, A.A. Balkema, Rotterdam, pp. 509-565.

Vesic, A.S. (1975). Bearing Capacity of Shallow Foundations. Winterkorn, H.F. & Fang, H.Y. (eds) Foundation Engineering Handbook, Van Nostrand Reinhold, New York, pp. 121-147.

List of Symbols

A: area of footing
A_c: area of the cemented layer
A_s: area of the steel plate
c': effective cohesion intercept
D: diameter of the circular steel shallow foundation
D_r: diameter of the circular sand-Portland cement field layers
f_s: CPT sleeve friction
H_r: thickness of the sand-Portland cement field layers
L_r: width of the square sand-Portland cement field layers
q_c: CPT tip strength
q_0: bearing capacity of spread footing was resting on soil
N_c, N_q and N_γ: bearing capacity factors
Q: applied load
Q_u: failure load
S_c, S_q and S_γ: shape factors
δ: vertical displacement
δ/D or δ/D_r: relative displacement
ε_a: axial strain
ε_v: volumetric strain
σ_{eq}: equivalent pressure at the base of the cemented layer
ϕ': effective friction angle